Graphical Abstract

A novel catalytic system composed of mussel inspired adhesive moiety, catechol in combination of iron oxide nanoparticles, which could generate •OH in the presence of oxygen at pH 7.4. •OH could efficiently trigger various acrylate monomer polymerization and bilayer hydrogels were obtained in-situ. Notably, the incorporation of IONPs significantly enhanced mechanical properties of hydrogels.

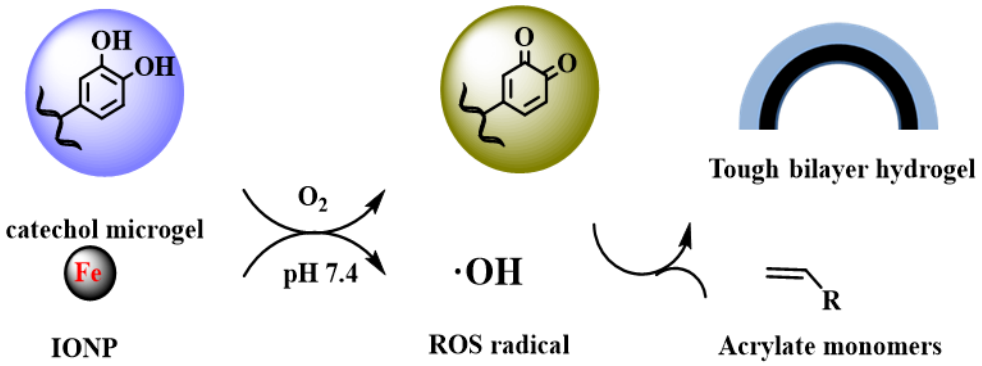

Highlights

1. A novel catalytic polymerization system composed of iron oxide magnetic nanoparticles and catechol containing microgels was reported.
2. The system initiated the polymerization of a wide ranges of monomers in an oxygenated aqueous solution.
3. Bilayer hydrogels were formed in-situ and the mechanical properties of these hydrogels were also improved.

Acrylate monomer polymerization triggered by iron oxide magnetic nanoparticles and catechol containing microgels

Bo Liu,[a,b] Zhongtian Zhang,[b] Bingqian Li,[a] Qingping Liu[a] and Bruce P. Lee[b]*

[a] Key Laboratory of Bionic Engineering (Ministry of Education, China), Jilin University, Changchun, Jilin 130022, China

[b] Department of Biomedical Engineering, Michigan Technological University, Houghton, Michigan 49931, United States

E-mail: bplee@mtu.edu

ABSTRACT: Phenol and its derivatives are the most used polymerization inhibitors for vinyl-based monomers. Here, we reported a novel catalytic system composed of mussel inspired adhesive moiety, catechol, in combination with iron oxide nanoparticles (IONPs) to generate hydroxyl radical (•OH) at pH 7.4. The generated •OH efficiently triggered free radical polymerization of various water-soluble monomers. Compared with the typical free radical initiating systems, the reported system does not require the addition of extra initiators for polymerization. During the process of polymerization, a bilayer hydrogel was formed *in situ* and exhibited the ability to bend during the process of swelling. The incorporation of IONPs significantly enhanced magnetic property of the hydrogel and the combination of DHM and IONPs also improved the mechanical properties of these hydrogels.

Keywords: catechol, iron oxide, free radical polymerization, bilayer hydrogels, in-situ.

20

21 **1. Introduction**

22 Phenolic compounds are the most used inhibitors for free radical polymerization of vinyl- and
23 acrylate-based monomers.[1-3] These phenolic compounds usually work together with molecular
24 oxygen to react with polymer alkyl radicals produced by the initiator and forms peroxy radicals.
25 The phenolic hydroxyl groups are susceptible to integrate with peroxy radicals to form the more
26 stable radicals that terminate peroxy radicals.[4] This inhibition property is affected by the number
27 of phenolic hydroxyl groups and electronic effect of aromatic substituents.[5] Catechol, an
28 adhesive moiety found in mussel adhesive proteins, is a phenolic compound consisting of two
29 hydroxyl groups in the ortho position.[6-9] Catechol is a well-known inhibitor and can react with
30 the initiating radical through the formation of aryloxy free radicals.[10-12] Hence, the protecting
31 groups like methoxy, borax, triethylsilyl, acetal *etc.* are often employed to chemically modify
32 catechol to during the process of free-radical initiated polymerization.[13, 14]
33 Catechol can generate various types of reactive oxygen species (ROS) during different oxidation
34 conditions such as autoxidation, chemical-mediated oxidation, and metal ion-mediated
35 oxidation.[15-17] ROS are highly reactive radicals and non-radical derivatives formed from
36 molecular oxygen. Common ROS are superoxide ($\bullet O_2^-$), singlet oxygen ($^1O_2$), hydrogen peroxide
37 (H_2O_2), and hydroxyl radical (•OH).[18] Catechol generates $\bullet O_2^-$ during autoxidation, which can
38 be further converted into H_2O_2 under basic condition.[19, 20] During iron oxide nanoparticles
39 (IONPs) mediated catechol oxidation, $\bullet O_2^-$ can be converted into $^1O_2$ at both acidic and basic pH
40 ranges.[17] •OH is a highly reactive and potent oxidant. •OH can be produced by converting
41 catechol-generated H_2O_2 in the presence of iron containing compound such as hematin via a

42 Fenton-like reaction.[21] These ROS can be used for organic compound degradation, cancer
43 therapy, and antimicrobial applications.[22]
44 Here, we seek to exploit a metal-catechol two-component catalytic polymerization system that can
45 produce the highly active ROS for free radical polymerization (Figure 1). In this design, catechol-
46 containing microgel is used as the source of ROS generation. Catechol converts molecular O_2 in
47 an aqueous solution into $\bullet O_2^-$ and H_2O_2, successively, through autoxidation when the microgels
48 were hydrated. The generated ROS can be further converted to •OH by IONPs through reacting
49 with $\bullet O_2^-$ via the Haber−Weiss reaction or H_2O_2 via the Fenton reaction. As such, catechol and
50 IONPs can form the redox polymerization initiators, which can catalyze the polymerization of
51 various acrylate monomers into mechanically strong and highly stretchable hydrogels. More
52 interestingly, the formed hydrogels were divided into two layers due to the settling of the microgel
53 and IONPs. The layer thicknesses, actuation, and mechanical property of these hydrogels could be
54 tuned with the content of IONPs. Finally, magnetic properties of the bilayer hydrogels were also
55 investigated.

56 **2. Materials and methods**

57 **2.1. Materials**

58 IONPs, acrylamide (AM), methyl acrylamide (MAM), [2-
59 (methacryloyloxy)ethyl]trimethylammonium chloride (METAC), [2-
60 (methacryloyloxy)ethyl]dimethyl-(3-sulfopropyl)ammonium hydroxide (SBMA), 1-vinyl-2-
61 pyrrolidone (N-VP), N-Hydroxyethyl acrylamide (HEAA), 2-hydroxyethyl methacrylate
62 (HEMA), 2-acrylamido-2-methyl-1-propanesulfonic acid (AMPS), 2-acrylamido-2-methyl-1-
63 propanesulfonic acid sodium salt solution (AMPS-Na), acrylic acid (AA), N-isopropylacrylamide
64 (NIPPAM), 4-acryloylmorpholinen (AMP) 4-vinylbenzenesulfonic acid (VBS) and 2-acrylamido-

65 2-methyl-1-propanesulfonic acid (AMPS) were purchased from Sigma-Aldrich. 2,2'-Azobis(2-
66 methyl-N-(2-hydroxyethyl)propionamide) were purchased from FUJIFILM Wako Pure Chemical
67 Corporation. Polyethylene glycol dimethacrylate-8K (PEGDMA) was purchased from polymer
68 science. Phosphate buffer saline (PBS), ferrous oxidation−xylenol orange (FOX) Assay Kit,
69 hydroxyphenyl fluorescein (HPF) and dihydroethidium (DHE) were purchased from Thermo
70 Fisher Scientific.

71 **2.2. Hydrogel preparation by DHM and IONPs**

72 Described below is the procedure for the synthesis of AP-1 hydrogel with AM and PEGDMA.
73 Other monomer-based hydrogels were prepared using a similar procedure. AM (0.355 g, 5 mmol),
74 PEGDMA (20.0 mg, 2.5 x 10^{-3} mmol) were first dissolved by 1 mL PBS (pH = 7.4) in a 5 mL vial.
75 After that, DHM (20.0 mg) and IONPs (20.0 mg) were added into the solution and use the vortex
76 for disperse the solution for 1 min. The mixture was put into the oven, which was set as 70 ^{o}C. The
77 solution fully changed to gel after 120 min. The hydrogel was flushed with deionized water 3-5
78 times. The mass of IONPs were 5 and 10 mg for AP-0.25 and AP-0.5, respectively.

79 **2.3. AP-0 Hydrogel preparation by 2,2'-azobis(2-methyl-N-(2-hydroxyethyl)propionamide)**

80 AM (0.355 g, 5 mmol), PEGDMA (20.0 mg, 2.5 x 10^{-3} mmol) were first dissolved by 1 mL PBS
81 (pH = 7.4) in a 5 mL vial. After that, 2,2'-azobis[2-methyl-N-(2-hydroxyethyl)propionamide] (20
82 mg, 0.069 mmol) were added into the solution and use the vortex for disperse the solution for 1
83 min. The mixture was put into the oven, which was set as 70 ^{o}C. The solution fully changed to gel
84 after 120 min. The hydrogel was flushed with deionized water 3-5 times.

85 **2.4. Methods**

86 **H_2O_2 characterization:** Twenty-five milligrams of DHMs (containing 10 mol % DMA) were
87 added to 1 mL pH 7.4 PBS with and without 25 mg IONPs to determine the generation of H_2O_2.
88 H_2O_2 generation was determined using FOX Assay Kit by following a published protocol using a
89 Synergy Mx microplate reader (BioTek, VT) [1].

90 **•OH characterization:** Twenty-five milligrams of DHMs were hydrated in 1 mL pH 7.4 PBS with
91 and without 25 mg IONPs. Three microliters of HPF (10 μM) were added to the microgel
92 suspension while protected from ambient light. The microgel suspension was incubated for up to
93 24 h at 37 °C (in the dark) with gentle agitation on a shaking plate. Microgels were separated by
94 centrifugation at 8000 rpm for 15 min and the fluorescence intensity was measured in the
95 supernatant solution using the same microplate reader above with an excitation/emission
96 wavelength of 490/528 nm.

97 **•O_2^- characterization:** All the procedures were kept the same as those used in hydroxyl radical
98 characterization besides two modifications. One modification was that HPF was replaced by DHE
99 without changing the concentration. The other modification was using an excitation/emission
100 wavelength of 518/606 nm for DHE detection.

101 **FTIR:** The transparent layers were cut off after the hydrogels were fully swollen. FTIR of the
102 lyophilized the transparent layers were tested on Shimadzu IRTracer-100 spectrometer.

103 **FE-SEM and EDX:** To image the network morphology, hydrogels were freeze-dried, coated
104 with platinum, and imaged using a FE-SEM in conjunction with EDX spectroscopy. (FE-SEM,
105 HITACHI S-4700).

Swelling ratio: Lyophilized hydrogels (diameter × height = 10 mm × 2.5 mm) were incubated in pH 3, pH 7.4 and pH 9 at 25 °C for up to 24 h. The mass of hydrogels in the swollen (W_s) and dried (W_d) states were used to determine the swelling ratio (SR) as calculated by: $SR = (W_s - W_d)/W_d \times 100\%$.

Finite Element Simulations: Finite element simulations were conducted to predict and verify the shape evolution of the double-layered structures by using the commercially available finite element software ABAQUS (Dassault Systems). The geometrical configurations of simulation models were identical as that of the samples in the experiment. For both the black layer and the transparent layer, elastic modulus is kept constant, and the swelling ratio is the only variable and change over time. The shape morphing is predicted by the principle of thermal expansion, and the predefined thermal field could be utilized to tune the deforming curvature.

Stimuli-responsive shape transformations of bilayer hydrogels: The bilayer hydrogel was cut into strips (length × height × width = 30 mm × 2.5 mm × 2.5 mm) and equilibrated in DI water at 25 ^{o}C for 24 h. The shape transformation of the hydrogel in these environments was recorded using iPhone 8. The bending angle of the bilayer hydrogel in the digital photo was measured, and the curve of bending angle versus time was plotted.

Magnetic property of hydrogels: The magnetic properties of the hydrogels were observed visually with a magnet, and their magnetization was measured accurately using a vibrating sample magnetometer (VSM) (PPMS-9, Quantum Design, USA) at 300 K. The range of the applied magnetic field strengths was from −60 kOe to 60 kOe. The saturation magnetization and the coercivity were determined.

127 **Rheometry:** The rheological properties of the hydrogels were examined using a TA Discovery
128 Hybrid Rheometer-2. A cone-and-plate geometry with a 20 mm diameter plate, and 3 mm gap was
129 used for all experiments on hydrogels. Hydrogels (diameter = 20 mm, thickness = 2.5 mm) were
130 equilibrated in DI water with nutation for 48 h. The modulus was determined at an oscillatory
131 strain range of 0.1% to 500% at a constant frequency (f) of 0.1 Hz.

132 **Tensile:** The tensile test was performed on MTS-1025638 (MTS Systems Corporation). The
133 long strip samples (length × height × width = 30 mm × 2~2.5 mm × 6 mm) with a gap length of 5
134 mm were stretched at a crosshead speed of 0.41667 mm/s. Tensile strain = $(l - l_0/l_0) \times 100\%$,
135 where l is the stretch length and l_0 is the gap length. Tensile stress = F/S (Pa), where F is the
136 tensile force and S is the square of original cross-sectional area.

137 **Compression:** Compressive stress-strain of hydrogels (diameter = 4 mm, thickness = 5 mm) were
138 obtained by a mini compression test machine (Bose ELF3200, USA). The compression test was
139 operated with a load cell of 10 N, the compression velocity was 0.1 mm/s. The stress and strain
140 values presented were taken from 0% to 80% compressive strain.

141 **3. Results and discussions**

142 Catechol-containing microgels were prepared by copolymerizing dopamine methacrylamide
143 (DMA) with HEAA microgels (DHM) following published protocol.[20] To initiate free-radical
144 polymerization, DHM and IONPs were added to a precursor solution containing a monomer, AM,
145 and a crosslinker, PEGDMA, in PBS (pH 7.4) (Figure 1(a)). The precursor solution solidified to
146 form black and compact hydrogel after 120 min (Figures 1(b) and 1(c)). Interestingly, the whole
147 polymerization process did not require removal of molecular oxygen from the reaction mixture.
148 Due to the magnetic nature of IONPs, the obtained hydrogel could be easily abstracted by a magnet

149 (Figure 1(d)). FTIR spectra of hydrogels exhibited the characteristic peaks at 3320 and 1620 cm^{-1}

150 for AM that are associated with $-NH_2$ and phenol -C=O stretching groups, respectively (Figure

151 S1).

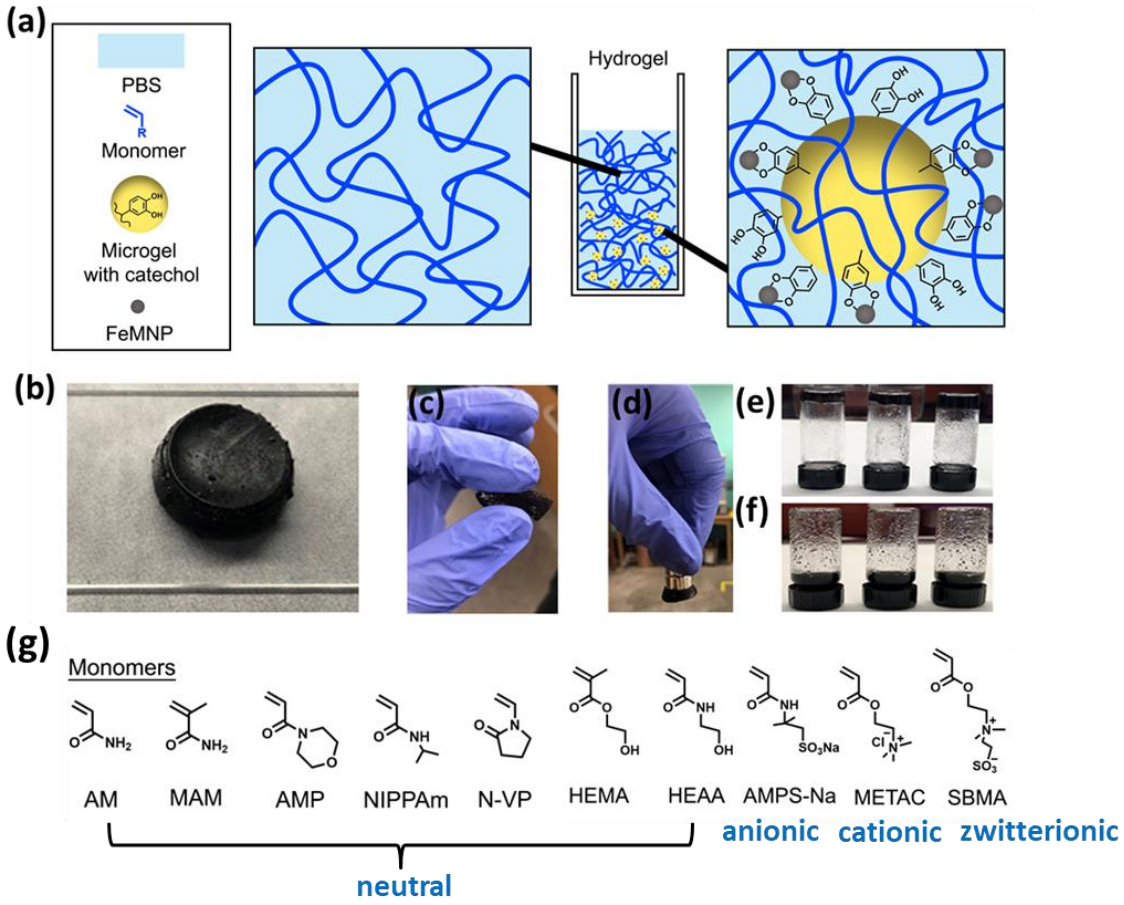

152

153 **Figure 1.** (a) Schematic of hydrogels formation by IONPs and DMA/HEAA microgels, (b)

154 overhead, (c) cross-section and (d) magnetic attraction of the resulting hydrogel, vial inversing

155 testing for (e) AM, HEMA, NIPPAM and (f) AA, VBS and AMPS, (g) Applicable monomers for

156 this catalytic system.

157

158 Various water-soluble acrylate monomers including neutral monomers (AM, MAM, AMP,
159 NIPPAm, N-VP, HEMA, HEAA), anionic monomer (AMPS-Na), cationic monomer (METAC),
160 and zwitterionic monomer (SBMA) were polymerized in the presence of DHM and IONPs, which
161 confirmed the applicability of this catalytic system. However, anionic monomers without counter
162 ions such as AA with a carboxylic acid group and 4-vinylbenzenesulfonic acid (VBS) or 2-
163 acrylamido-2-methyl-1-propanesulfonic acid (AMPS) with a sulfonic acid group did not
164 polymerize using the same reaction condition (Figure 1(f)). This is mainly due to the pH change
165 of the precursor solution to an acidic condition. Similarly, when the precursor solution pH was
166 adjusted to pH 3, all the monomers (Figure 1(g)) did not polymerize. This indicated that the
167 polymerization only occurred in the basic solution, which is necessary to promote catechol
168 autoxidation and ROS generation.[23] Using a catechol-free HEAA microgel in combination with
169 IONPs or DHM without INOP did not initiate polymerization. Therefore, the combination of
170 catechol, iron, and pH were directly responsible for hydrogel formation.
171 The amount of $\bullet O_2^-$, H_2O_2 and •OH generated by DHM with and without IONPs were determined
172 by using DHE, FOX assay, and HPF assay, respectively (Figure 2). Upon hydration, DHM started
173 to generate $\bullet O_2^-$ and the DHE fluorescence intensity was around 150 after 15 min and remained
174 unchanged over 180 min. O_2 oxidizes catechol to semiquinone and quinone, while generating $\bullet O_2^-$
175 by one-electron oxidation of catechol during the hydration.[24] Meanwhile, H_2O_2 was also
176 detected from DHM. Concentration of H_2O_2 increased over time and reached a maximum
177 concentration of around 2100 μM after 180 min. The H_2O_2 release profile was consistent with
178 previously published report.[23] $\bullet O_2^-$ is generated during catechol oxidation, which further reacted
179 with protons in the solution to form H_2O_2. However, •OH was not detected from DHM.

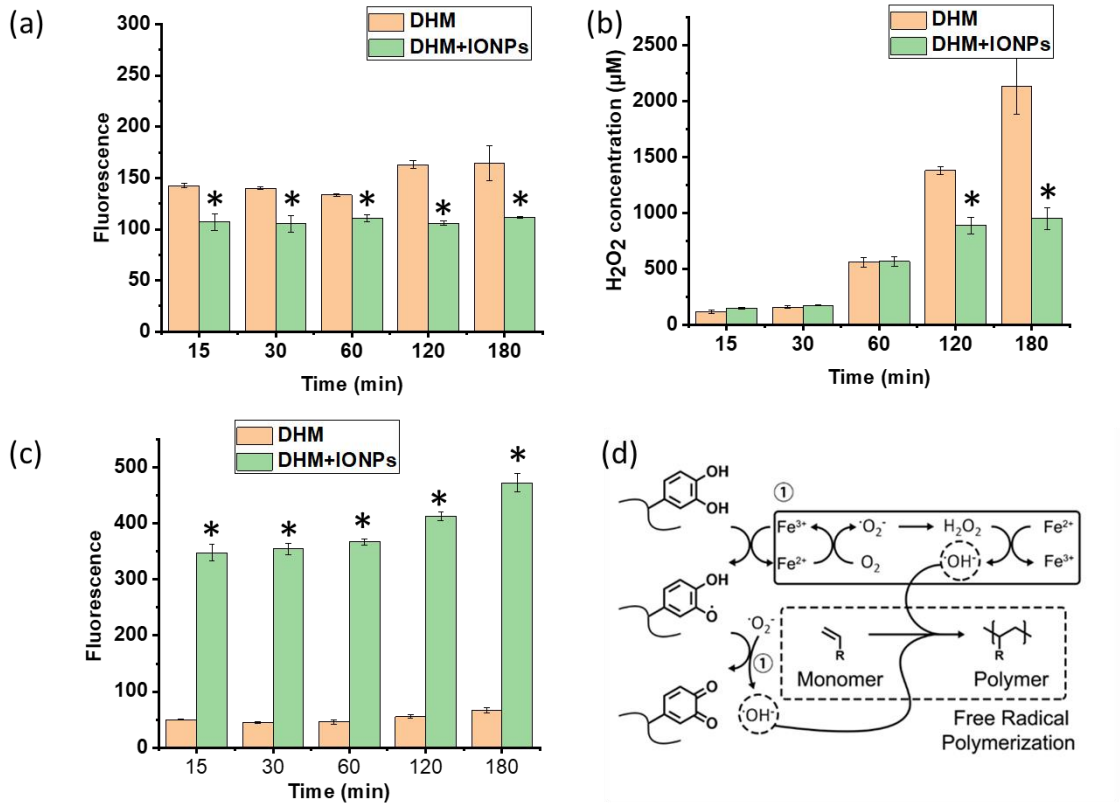

Figure 2. (a) H_2O_2 generation, (b) $\bullet O_2^-$ detection using DHE probe, (c) •OH detection using HPF probe from microgels or microgels with IONPs hydrated in PBS with different time, (d) proposed mechanism of polymerization. * $p < 0.05$ when compared to DHM with different time.

When both DHM and IONPs were incubated together, there was a marked reduction in the amount of $\bullet O_2^-$ and H_2O_2 that were detected when compared to DHM alone. However, the HPF fluorescence intensity increased over 7 folds with the addition of IONPs. This clearly indicated that the generated $\bullet O_2^-$ and H_2O_2 were converted to •OH in the presence of the iron metal. Catechol was first oxidized by Fe^{3+} to form a semiquinone radical intermediate. $\bullet O_2^-$ was obtained by the O_2 reduction of semiquinone and Fe^{2+}. Subsequently, $\bullet O_2^-$ was further reduced to H_2O_2, which is further reduced by Fe^{2+} to produce •OH (Figure 2(d)). •OH was the main initiator that induced the polymerization of the various monomers.

192 The effect of the mass ratio between IONPs and DHM (0.25:1, 0.5:1, and 1:1 denoted as AP-0.25,
193 AP-0.5, and AP-1, respectively) on the formation of the cured hydrogel was further investigated
194 using AM as the monomer and PEGDMA as the crosslinker (Table S1). All the three hydrogels
195 were formed after 120 min of polymerization. For comparison purposes, the control hydrogel (AP-
196 0) was formed through polymerization using 2,2'-azobis(2-methyl-N-(2-hydroxyethyl)
197 propionamide) at 70 ^{o}C without IONP and DHM. Interestingly, AP-0.25, AP-0.5, and AP-1 formed
198 bilayer structures consisting of a transparent upper layer and a black bottom layer, while the control
199 hydrogel AP-0 was the homogenous transparent layer (Figure 3(a)). The bilayer hydrogels formed
200 due to settling of IONPs and DHM due to the hydrophobic nature of IONPs and non-water
201 solubility of microgels when the polymerization began. The monomers were polymerized
202 immediately adjacent to the settled DHM and IONPs given the proximity to the catalyzing
203 moieties. The transparent top layer also formed a crosslinked hydrogel, indicating that the chain
204 propagation did not need to occur near the catalytic DHM and IONPs.
205 The microstructures of these hydrogels were also confirmed by FE-SEM) (Figure 3. The control
206 AP-0 exhibited a homogenous network structure typical of a crosslinked hydrogel. Hydrogels
207 initiated by DHM and IONPs exhibited a bottom black layer and the thickness of this black layer
208 increased with increasing INOP content. The black layer thickness in AP-1 was about 2.2 times
209 and 1.3 times thicker when compared to those of AP-0.25 and AP-0.5 due to the higher IONPs
210 content in AP-1 (Figure 3(c) (i), Figure 3(d) (i) and, Figure 3(e) (i)). Moreover, the spherical
211 microgels were embedded into the black layers (Figure 3(c) (ii), Figure 3(d) (ii) and, Figure 3(e)
212 (ii)). The transparent upper layers did not contain any microgels or IONPs and resembled porous
213 network structure of a hydrogel. Energy-dispersive X-ray spectroscopy (EDX) analysis of AP-1
214 demonstrated that Fe elements from IONPs were distributed around the microgels in the black

215 layer (Figure S2). No Fe element was detected in the transparent layer. This indicated that IONPs

216 were attached to the surface of the microgels because of catechol's affinity for Fe.

217

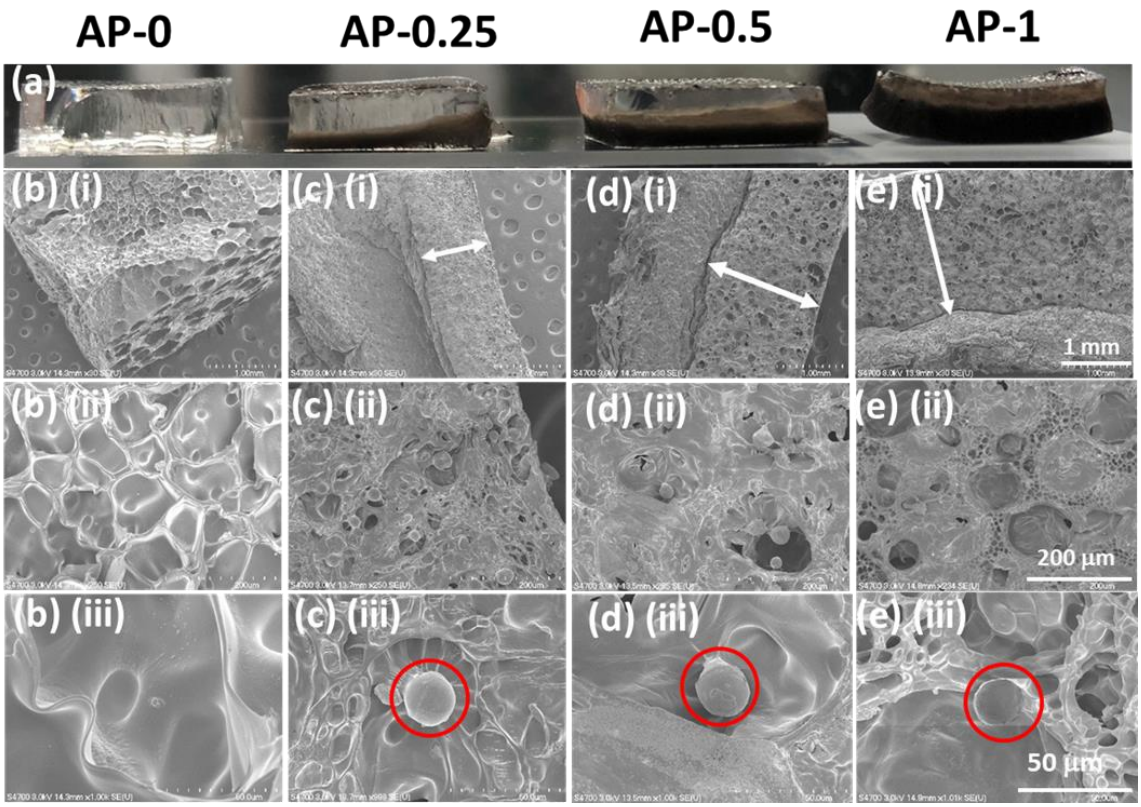

218 **Figure 3.** (a) Optical images of hydrogels and FE-SEM images of (b) AP-0, (c) AP-0.25, (d) AP-

219 0.5, and (e) AP-1 at (i) 30×, (ii) 250×, and (iii) 1000× magnification. (ii) and (iii) images for column

220 (c), (d), and (e) are images of the black layer for DHM and IONPs initiated hydrogels. The double-

221 sided arrows indicate the bottom, black layer of the hydrogel and the red circles indicate DHM.

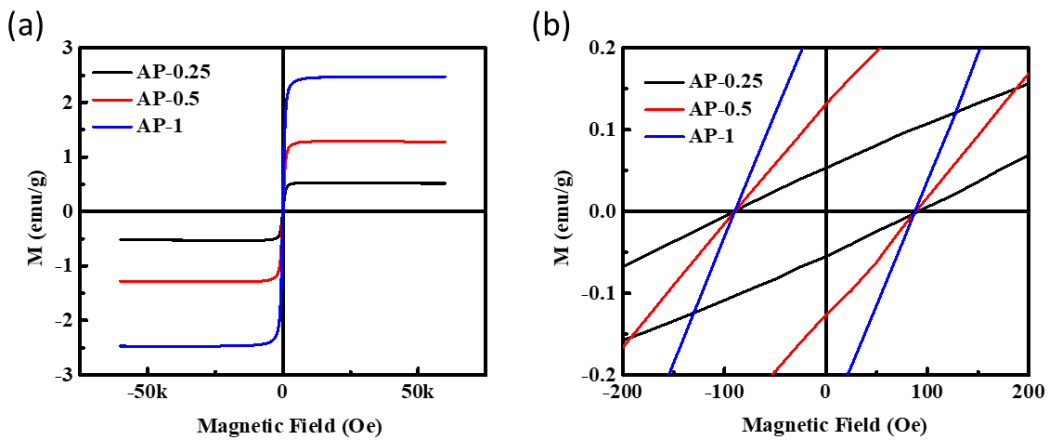

Figure 4. (a) Saturation magnetization values and (b) magnetic hysteresis loops of AP-0.25, AP-0.5 and AP-1 at 300 K.

The magnetic properties of hydrogels were measured by VSM with a magnetic field range of −60 kOe to 60 kOe at 300 K (Figure 4). The saturation magnetization values for AP-0.25, AP-0.5, and AP-1 were 2.47, 1.28 and 0.52 emu/g, respectively (Figure 4). As expected, the magnetic intensity of the hydrogels increased with increasing content of IONPs. The hysteresis loop was from −0.1 kOe to 0.1 kOe, indicating that very low energy is required to reverse the magnetization.

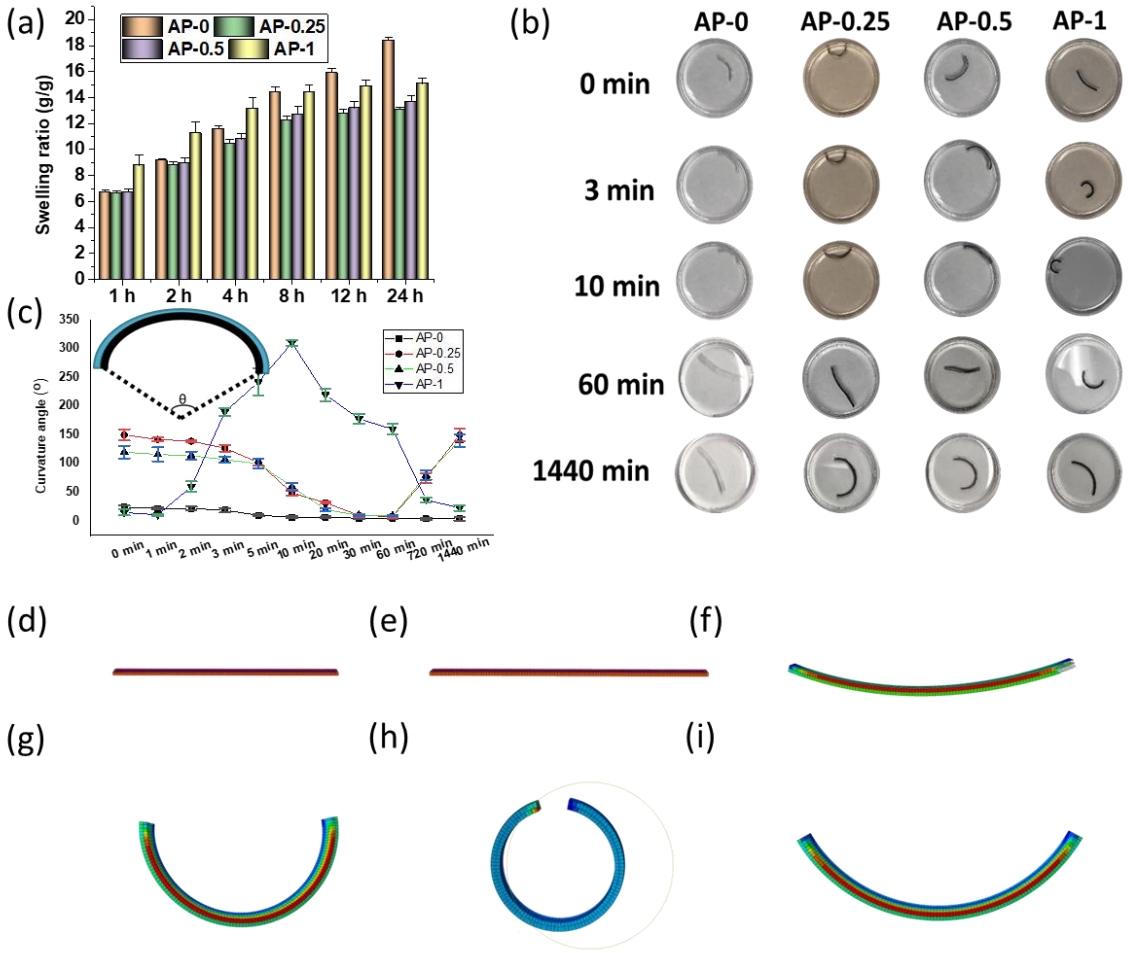

Figure 5. (a) The swelling ratios; (b) images; and (c) the curvature angels of hydrogels equilibrated in deionized water for different time. Deformation simulation of (d-e) AP-0 and (f-i) AP-1 using Abaqus.

The swelling ratios of hydrogels were around 13 to 18 after incubating the deionized water for 24 h. AP-0 exhibited the largest swelling ratio (18.2) since the hydrogel was consisted of hydrophilic AM and PEGDMA. Swelling ratios for AP-0.25, AP-0.5, and AP-1 were 12.5, 13.2 and 14.1, respectively; because the more hydrophobic DHM and IONPs were embedded within the black layers (Figure 5(a)). Due to the swelling ratio differences within the bilayers, the dry AP hydrogels

had an outward bend, arching the black layers of the materials after equilibrated in the deionized water (Figure 5(b)). Especially for AP-1, the curvature angel can reach up to 300° after 10 min of incubation. Water entered the porous structures in the black layers more easily, which was also consistent with 1 h swelling ratio results. As the swelling continued, the transparent layer absorbed more water than the black layer. As such, the curvature angel gradually decreased, and was only 45° after 24 h incubation (Figure 5(c)). Abaqus was used to simulate the deformation of AP-0 and AP-1. The results indicated that AP-0 remained mostly undeformed, while AP-1 deformed in the similar manner with the experiment results (Figure 5(d)-5(i)).

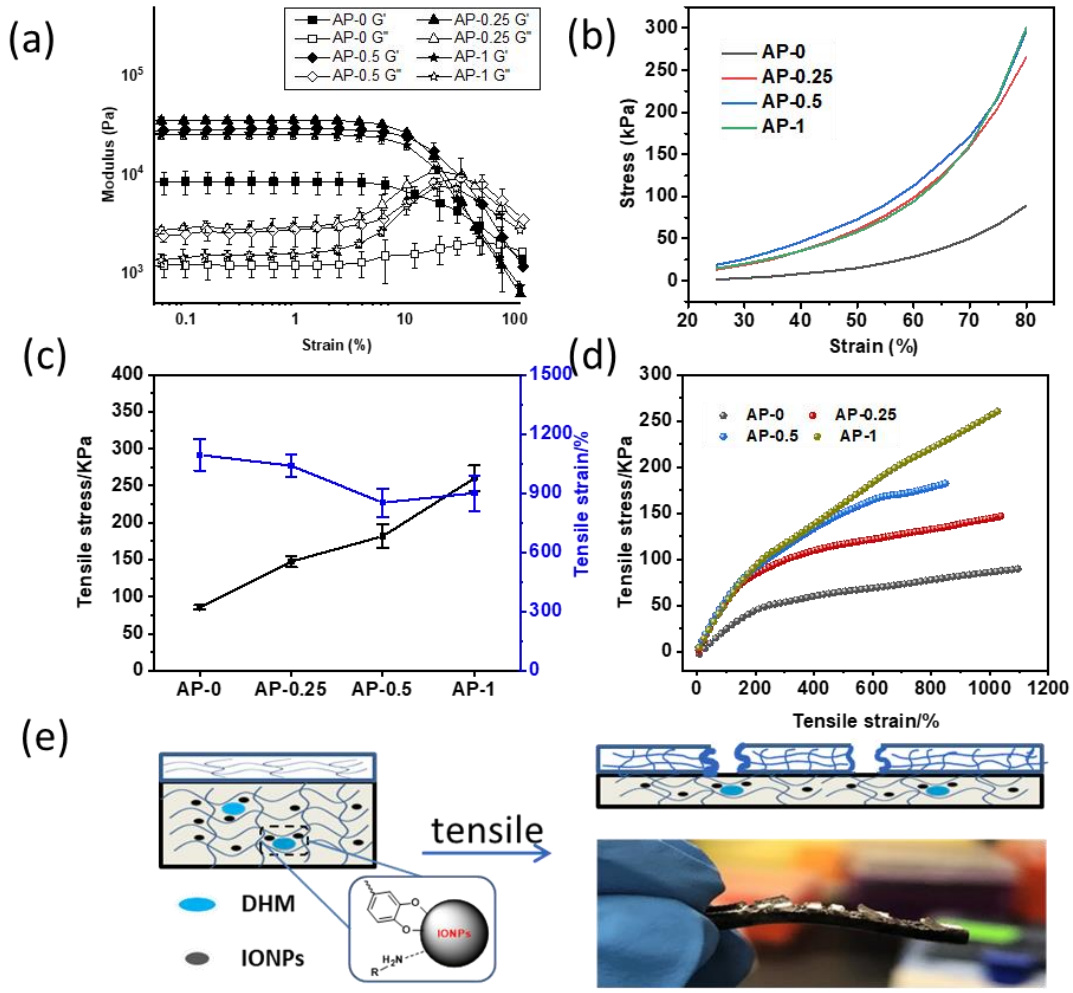

248 **Figure 6.** Mechanical properties of AP-X hydrogels. (a) Storage (G′, filled symbol) and loss (G″,
249 open symbol) moduli, (b) compressive stress–strain curves, (c), (d) tensile stress and tensile strain
250 curves of AP-X hydrogels, (e) fracture mode of AP-0 AP-0.25, AP-0.5 and AP-1.

251 The mechanical property of AP hydrogels was also investigated. The storage modulus (G') value
252 was 1 order of magnitude higher than the loss modulus (G") in all cases, indicating that all the
253 hydrogels were fully crosslinked. IONPs-containing hydrogels (AP-0.25, AP-0.5, and AP-1)
254 exhibited higher G' values in the linear viscoelasticity regions when compared to that of the
255 IONPs-free hydrogel AP-0 (Figure 6(a)). Similarly, the compression modulus of AP-0.25, AP-0.5,
256 and AP-1 were 300.0, 295.7, and 265.4 kPa, all of which were much higher than 88.9 kPa of AP-
257 0 at the compression strain of 80% (Figure 6(b)). Interestingly, AP-1 recovered automatically and
258 rapidly to its original cylindrical shape over the multiple compressive cycles (Movie S1 and Figure
259 S3).
260 Figures 6(c) and 6(d) shows the typical tensile stress−strain curves of the hydrogels in uniaxial
261 tensile tests at a speed of 120 mm min^{-1}. IONPs free AP-0 exhibited a maximum tensile strain of
262 1094%, which was about 150% higher than IONPs containing hydrogels (Figure S4). The
263 maximum tensile stress increased significantly with increasing IONPs content. Maximum tensile
264 stress of AP-1 was 260 kPa, which was more than three times higher than that of AP-0 (85 kPa).
265 It indicated the incorporation of DHM and IONPs improved the mechanical strength of these
266 hydrogels only with a little sacrifice of elasticity because of the chelation effect between iron ions,
267 catechol and amide moieties. The decreasing of elasticity was also agreed with the rheometry
268 results. Notably, the bilayer hydrogel, AP-1 was fractured at the upper, transparent layer rather
269 than the black layer potentially due to the higher strength of this layer (Figure 6(e)). Overall, the
270 incorporation DHM and IONPs into hydrogels can lead to an increase in shear storage modulus,

271 compression modulus and tensile strength when compared to the control hydrogel. Both DHM and
272 IONPs functioned as fillers and chemical crosslinkers to improve the mechanical property of
273 hydrogels.
274 Taken together, we combined the polymerization inhibitors catechol and O_2 with IONPs, to create
275 a new redox initiator that can generate a highly reactive ROS, •OH. •OH was generated by IONPs-
276 catalyzed oxidation of catechol and effectively initiate various acrylate monomers polymerization
277 via a Fenton-like reaction. Compared with the typical free radical initiating systems, no extra
278 initiators such as photo- or thermal initiators were required for polymerization. Unlike the other
279 existing metal-catechol polymerization system[25-28], this presented polymerization occurred in
280 a mild aqueous condition and without requiring additional source to generate free radicals. This
281 differs from recent reports that combined metal ions (Fe^{3+} and Ag^{+}) and catechol while using
282 ammonium persulfate (APS) as added source of free radicals to initiate polymerization.[25] During
283 the process of polymerization, DHM and IONPs settled to the bottom of the reaction mixture to
284 generate bilayer hydrogel actuator. Comparing with the existing bilayer hydrogels which were
285 usually fabricated in a two-step method[29, 30] or with some other supplementary device[31, 32],
286 the recipe presented in this work was much simpler and tunable. The thickness of the two layers
287 can be easily adjusted by altering the content of IONPs. In addition, the incorporation of DHM
288 and IONPs into AM-based hydrogels exhibited an increase of mechanical properties. The novel
289 catalytic polymerization system by using the catechol and IONPs provides a basis for designing a
290 novel functional bilayer hydrogel that can feature as the actuators with programmable and versatile
291 properties for many smart soft material applications.

292 **4. Conclusion**

293 In conclusion, a novel catalytic polymerization system composed of IONPs and catechol
294 containing microgels was reported. This combination initiated the polymerization of a wide ranges
295 of monomers to form a hydrogel network in an oxygenated aqueous solution. Oxidation of catechol
296 generated $\bullet O_2^-$ and H_2O_2, which was subsequently converted into •OH by IONPs in the presence
297 of O_2. Bilayer hydrogels were formed *in situ* and exhibited the ability to bend during the process
298 of swelling. The incorporation of IONPs significantly enhanced magnetic property of the hydrogel
299 and the combination of DHM and IONPs also improved the mechanical properties of these
300 hydrogels.

301 **Acknowledgment**

302 This project was supported by the Office of Naval Research under award number N00014-20-1-
303 2230, the National Science Foundation under award numbers DMR 2001076, and the National
304 Institutes of Health under award number R15GM135875.

305 **Appendix A. Supplementary data**

306 Supplementary data to this article can be found online at

307

References

[1] F. Lartigue-Peyrou, The use of phenolic compounds as free-radical polymerization inhibitors, in: J.-R. Desmurs, S. Ratton (Eds.), Industrial Chemistry Library, Elsevier1996, pp. 489-505. https://doi.org/https://doi.org/10.1016/S0926-9614(96)80036-0.

[2] L.B. Levy, Inhibition of acrylic acid polymerization by phenothiazine and p-methoxyphenol, Journal of Polymer Science: Polymer Chemistry Edition 23(5) (1985) 1505-1515. https://doi.org/https://doi.org/10.1002/pol.1985.170230522.

[3] Tüdo, x030B, F. s, T. Földes-Berezsnich, Free-radical polymerization: Inhibition and retardation, Progress in Polymer Science 14(6) (1989) 717-761. https://doi.org/https://doi.org/10.1016/0079-6700(89)90008-7.

[4] V.A. Bhanu, K. Kishore, Role of oxygen in polymerization reactions, Chemical Reviews 91(2) (1991) 99-117. https://doi.org/10.1021/cr00002a001.

[5] S. Nagarajan, R. Nagarajan, J. Kumar, A. Salemme, A.R. Togna, L.A.-O. Saso, F. Bruno, Antioxidant Activity of Synthetic Polymers of Phenolic Compounds. LID - 10.3390/polym12081646 [doi] LID - 1646, (2073-4360 (Electronic)).

[6] B.K. Ahn, Perspectives on Mussel-Inspired Wet Adhesion, Journal of the American Chemical Society 139(30) (2017) 10166-10171. https://doi.org/10.1021/jacs.6b13149.

[7] P. Kord Forooshani, B.P. Lee, Recent approaches in designing bioadhesive materials inspired by mussel adhesive protein, Journal of Polymer Science Part A: Polymer Chemistry 55(1) (2017) 9-33. https://doi.org/https://doi.org/10.1002/pola.28368.

[8] B.P. Lee, P.B. Messersmith, J.N. Israelachvili, J.H. Waite, Mussel-Inspired Adhesives and Coatings, Annual Review of Materials Research 41(1) (2011) 99-132. https://doi.org/10.1146/annurev-matsci-062910-100429.

[9] V. Mogal, V. Papper, A. Chaurasia, G. Feng, R. Marks, T. Steele, Novel On-Demand Bioadhesion to Soft Tissue in Wet Environments, Macromolecular Bioscience 14(4) (2014) 478-484. https://doi.org/https://doi.org/10.1002/mabi.201300380.

[10] R.G. Caldwell, J.L. Ihrig, The Reactivity of Phenols toward Peroxy Radicals. I. Inhibition of the Oxidation and Polymerization of Methyl Methacrylate by Phenols in the Presence of Air, Journal of the American Chemical Society 84(15) (1962) 2878-2886. https://doi.org/10.1021/ja00874a006.

[11] K.K. Georgieff, Relative inhibitory effect of various compounds on the rate of polymerization of methyl methacrylate, Journal of Applied Polymer Science 9(6) (1965) 2009-2018. https://doi.org/https://doi.org/10.1002/app.1965.070090602.

[12] N. Jiménez, F. Ruipérez, E. González de San Román, J.M. Asua, N. Ballard, Fundamental Insights into Free-Radical Polymerization in the Presence of Catechols and Catechol-Functionalized Monomers, Macromolecules 55(1) (2022) 49-64. https://doi.org/10.1021/acs.macromol.1c02103.

[13] E. Faure, C. Falentin-Daudré, C. Jérôme, J. Lyskawa, D. Fournier, P. Woisel, C. Detrembleur, Catechols as versatile platforms in polymer chemistry, Progress in Polymer Science 38(1) (2013) 236-270. https://doi.org/https://doi.org/10.1016/j.progpolymsci.2012.06.004.

[14] N. Patil, C. Jérôme, C. Detrembleur, Recent advances in the synthesis of catechol-derived (bio)polymers for applications in energy storage and environment, Progress in Polymer Science 82 (2018) 34-91. https://doi.org/https://doi.org/10.1016/j.progpolymsci.2018.04.002.
[15] B. Kalyanaraman, C.C. Felix, R.C. Sealy, Semiquinone anion radicals of catechol(amine)s, catechol estrogens, and their metal ion complexes, Environmental Health Perspectives 64 (1985) 185-198. https://doi.org/10.1289/ehp.8564185.
[16] J. Yang, M.A. Cohen Stuart, M. Kamperman, Jack of all trades: versatile catechol crosslinking mechanisms, Chemical Society Reviews 43(24) (2014) 8271-8298. https://doi.org/10.1039/C4CS00185K.
[17] Z. Zhang, X. He, C. Zhou, M. Reaume, M. Wu, B. Liu, B.P. Lee, Iron Magnetic Nanoparticle-Induced ROS Generation from Catechol-Containing Microgel for Environmental and Biomedical Applications, ACS Applied Materials & Interfaces 12(19) (2020) 21210-21220. https://doi.org/10.1021/acsami.9b19726.
[18] H. Sies, D.P. Jones, Reactive oxygen species (ROS) as pleiotropic physiological signalling agents, Nature Reviews Molecular Cell Biology 21(7) (2020) 363-383. https://doi.org/10.1038/s41580-020-0230-3.
[19] H. Meng, Y. Li, M. Faust, S. Konst, B.P. Lee, Hydrogen peroxide generation and biocompatibility of hydrogel-bound mussel adhesive moiety, Acta Biomaterialia 17 (2015) 160-169. https://doi.org/https://doi.org/10.1016/j.actbio.2015.02.002.
[20] H. Meng, Y. Liu, B.P. Lee, Model polymer system for investigating the generation of hydrogen peroxide and its biological responses during the crosslinking of mussel adhesive moiety, Acta Biomaterialia 48 (2017) 144-156. https://doi.org/https://doi.org/10.1016/j.actbio.2016.10.016.
[21] P. Kord Forooshani, R. Pinnaratip, E. Polega, A.G. Tyo, E. Pearson, B. Liu, T.-O. Folayan, L. Pan, R.M. Rajachar, C.L. Heldt, B.P. Lee, Hydroxyl Radical Generation through the Fenton-like Reaction of Hematin- and Catechol-Functionalized Microgels, Chemistry of Materials 32(19) (2020) 8182-8194. https://doi.org/10.1021/acs.chemmater.0c01551.
[22] Q. Xu, C. He, C. Xiao, X. Chen, Reactive Oxygen Species (ROS) Responsive Polymers for Biomedical Applications, Macromolecular Bioscience 16(5) (2016) 635-646. https://doi.org/https://doi.org/10.1002/mabi.201500440.
[23] H. Meng, P.K. Forooshani, P.U. Joshi, J. Osborne, X. Mi, C. Meingast, R. Pinnaratip, J. Kelley, A. Narkar, W. He, M.C. Frost, C.L. Heldt, B.P. Lee, Biomimetic recyclable microgels for on-demand generation of hydrogen peroxide and antipathogenic application, Acta Biomaterialia 83 (2019) 109-118. https://doi.org/https://doi.org/10.1016/j.actbio.2018.10.037.
[24] D.T. Sawyer, J.S. Valentine, How super is superoxide?, Accounts of Chemical Research 14(12) (1981) 393-400. https://doi.org/10.1021/ar00072a005.
[25] D. Gan, W. Xing, L. Jiang, J. Fang, C. Zhao, F. Ren, L. Fang, K. Wang, X. Lu, Plant-inspired adhesive and tough hydrogel based on Ag-Lignin nanoparticles-triggered dynamic redox catechol chemistry, Nature Communications 10(1) (2019) 1487. https://doi.org/10.1038/s41467-019-09351-2.
[26] Z. Jia, Y. Zeng, P. Tang, D. Gan, W. Xing, Y. Hou, K. Wang, C. Xie, X. Lu, Conductive, Tough, Transparent, and Self-Healing Hydrogels Based on Catechol–Metal Ion Dual Self-Catalysis, Chemistry of Materials 31(15) (2019) 5625-5632. https://doi.org/10.1021/acs.chemmater.9b01498.

[27] A. Reyhani, T.G. McKenzie, Q. Fu, G.G. Qiao, Fenton-Chemistry-Mediated Radical Polymerization, Macromolecular Rapid Communications 40(18) (2019) 1900220. https://doi.org/https://doi.org/10.1002/marc.201900220.
[28] H.L. Bui, S.-D. Huang, B.P. Lee, M.-Y. Lan, C.-J. Huang, Catechol-functionalized sulfobetaine polymer for uniform zwitterionization via pH transition approach, Colloids and Surf., B 220 (2022) 112879. https://doi.org/https://doi.org/10.1016/j.colsurfb.2022.112879.
[29] J. Duan, X. Liang, K. Zhu, J. Guo, L. Zhang, Bilayer hydrogel actuators with tight interfacial adhesion fully constructed from natural polysaccharides, Soft Matter 13(2) (2017) 345-354. https://doi.org/10.1039/C6SM02089E.
[30] S. Xiao, M. Zhang, X. He, L. Huang, Y. Zhang, B. Ren, M. Zhong, Y. Chang, J. Yang, J. Zheng, Dual Salt- and Thermoresponsive Programmable Bilayer Hydrogel Actuators with Pseudo-Interpenetrating Double-Network Structures, ACS Applied Materials & Interfaces 10(25) (2018) 21642-21653. https://doi.org/10.1021/acsami.8b06169.
[31] N. Bassik, B.T. Abebe, K.E. Laflin, D.H. Gracias, Photolithographically patterned smart hydrogel based bilayer actuators, Polymer 51(26) (2010) 6093-6098. https://doi.org/https://doi.org/10.1016/j.polymer.2010.10.035.
[32] G. Qu, J. Huang, Z. Li, Y. Jiang, Y. Liu, K. Chen, Z. Xu, Y. Zhao, G. Gu, X. Wu, J. Ren, 4D-printed bilayer hydrogel with adjustable bending degree for enteroatmospheric fistula closure, Materials Today Bio 16 (2022) 100363. https://doi.org/https://doi.org/10.1016/j.mtbio.2022.100363.

Video

Click here to access/download

Video

movie s1.MOV